Catalysis Today 147S (2009) S99–S106

Contents lists available at ScienceDirect

Catalysis Today

journal homepage: www.elsevier.com/locate/cattod

Natural gas combustion catalysts for environmental-friendly domestic burners

Stefania Specchia [a,*], Giuseppe Toniato [b]

[a] Politecnico di Torino, Dipartimento di Scienza dei Materiali ed Ingegneria Chimica, Corso Duca degli Abruzzi 24, 10129 Torino, Italy
[b] Riello S.p.A., Via Ing. Pilade Riello 7, 37045 Legnago (VR), Italy

ARTICLE INFO

Article history:
Available online 31 July 2009

Keywords:
Methane combustion
Catalytic combustion
Perovskites
Mixed oxides
Domestic boiler
Premixed burners
Metal fibre mattress

ABSTRACT

The present work deals with the analysis of low-environmental-impact premixed metal fibre burners (Fe–Cr–Al fibre mats) for natural gas combustion, characterized by a satisfactorily combustion performance. In particular, perovskite- and mixed oxides-based catalysts, in synergism with Pd, were suitably developed at powder level and subsequently deposited over metal fibre mattress. New catalytic burners based on $LaMnO_3$-ZrO_2, CeO_2-ZrO_2, $BaCeO_3$-ZrO_2 and Pd/$LaMnO_3$-ZrO_2, Pd/CeO_2-ZrO_2, Pd/$BaCeO_3$-ZrO_2 catalysts were studied determining, first of all, the optimal operating conditions for catalysts preparation via the solution combustion synthesis (SCS). After preliminary investigations at powder level, the catalysts were then deposited over metal fibre mats to obtain premixed burners for household appliances. The resulting structured catalysts were then tested on a commercial domestic boiler under realistic operating conditions. The obtained results with the Pd-based catalytic burners showed better performances compared with those of the commercial burner, in terms of CO emissions. The NO emissions, however, resulted somehow increased, especially at the low thermal power rates and air excess, whereas they slightly decreased at high air excess. The most interesting results in terms of CO emission reduction were obtained with the Pd/CeO_2-ZrO_2 catalyzed burner.

1. Introduction

In accordance with the last climate policy (e.g. Kyoto protocol), reduction of HC, CO and NO_x emissions and increase of safety and efficiency in the natural gas (NG) combustion processes have recently become even more important since the demand of NG as energy source has been increasing worldwide. In the recent years, catalytic combustors for gas turbines and domestic appliances evolved from research level to field-testing and commercial scale [1], claiming lower NO_x, CO and unburned HC emissions than any other equivalent device relying on conventional combustion [2,3].

Among potential applications of this technology for energetic purposes, growing interest is focusing on the study of pre-mixed NG combustion items in non-adiabatic conditions, such as porous radiant burners for domestic and industrial applications [4–8] or to provide heat for endothermic chemical processes at high temperature, as dehydrogenation and steam reforming [9,10]. In the radiant premixed catalytic combustion technology, structured catalysts of various shapes, e.g., honeycomb, cloth, tube, particles or fibres, have been used. A pre-mixture of fuel and air introduced into the catalyst is burnt by both catalytic and gas-phase oxidation, radiating energy from the structured catalyst surface.

The best catalysts for CH_4/HCs combustion are those based on the noble metals as Pt and Pd [11], but because of their high and fluctuating cost, ways of minimizing their amount into the burners are sought. However, a wide implementation of such technologies still requires the development of economically acceptable, high performing catalysts with enhanced thermal stability. Perovskite-type mixed oxides were originally proposed as an attractive alternative to the very active noble metals Pt and Pd for their chemical and thermal stability and lower cost accompanied by a good specific activity at moderate temperature, but suffering from sintering effects at elevated temperatures [11–13]. Among the many perovskite compositions that can be considered, $LaMnO_3$ has been recognized having a remarkable effect in promoting the complete oxidation of CH_4 [14,15], although it presents relatively low specific surface area when it is synthesized via conventional preparation routes. In previous works of ours [7,8,16,17], it was demonstrated that the co-synthesis of $LaMnO_3$ and ZrO_2 gave a powder conserving both its morphology and catalytic activity, also after thermal ageing at very high temperature. Together with the previous one, two other catalysts were proposed in this work: the mixed oxide system CeO_2-ZrO_2 and the perovskite $BaCeO_3$ co-synthesized with ZrO_2. ZrO_2 acts as a structural promoter, in that its presence limits the specific surface area losses caused by

* Corresponding author. Tel.: +39 011 0904608; fax: +39 011 0904699.
E-mail address: stefania.specchia@polito.it (S. Specchia).

0920-5861/$ – see front matter © 2009 Elsevier B.V. All rights reserved.
doi:10.1016/j.cattod.2009.07.033

prolonged exposure to high temperatures [18]. CeO_2 is particularly appreciated as promoter for many utilizations in the catalytic combustion with noticeable application as automotive exhausts oxidation catalyst [19]. It shows, in fact, a good capability of changing rapidly its oxidation number from Ce^{3+} to Ce^{4+} state, with a consequent fast release of oxygen from its lattice to the reacting species [20,21]. The combustion synthesis of CeO_2 nanoparticles is also widely studied since 1990 [22], with a particular attention to obtain high surface area values [23]. The CeO_2-ZrO_2 production by co-synthesis is seen as a good method that should give a catalytic material with higher thermal stability respect to the simple oxide used as promoter in vehicle after treatment devices, where the working temperature are on average lower. The last proposed catalyst is the perovskite $BaCeO_3$ co-synthesized with ZrO_2. Such a perovskite is actually studied as storage-oxidation-reduction catalyst due to the presence of Ce as oxygen storage [20,24] and of BaO as electron donor [25].

Therefore, the present work deals with the analysis of the low-environmental-impact perovskite- and mixed oxides-based catalysts $LaMnO_3$-ZrO_2, CeO_2-ZrO_2 and $BaCeO_3$-ZrO_2, in synergism with Pd. All the prepared catalysts were fully characterized at powder level, without and with Pd. Then, all the catalysts were investigated in the structured form after deposition over premixed metal fibre burners on Fe–Cr–Al alloy fibre mats for household applications. To this goal, the resulting structured catalytic burners were tested on a commercial domestic boiler under realistic operating conditions and their performances were compared to those of the commercial, non-catalytic burner.

2. Experimental

2.1. Catalytic powders

All the catalysts proposed in this work were prepared by the Solution Combustion Synthesis (SCS) method. SCS, in fact, allows a rapid, economic and self-sustaining synthesis process based on the exothermic oxidation of an organic fuel like glycine [16,17]. The necessary heat for the catalytic materials formation is provided by the employed organic fuel [26]. First, catalysts without Pd were prepared: the metal nitrates (Aldrich, 99% purity) of Ce, La, Ba, and ZrO were used as precursors to co-synthesize the catalysts for their high solubility in water and since they act as oxidizers. The prepared aqueous solutions were poured in a crucible inserted in an oven kept at a constant temperature of about 450 °C. After water evaporation, the heat released in the fast reaction of nitrates reduction-organic fuel oxidation allowed the consequent formation of the catalytic powders. All the catalytic powders were calcinated after synthesis in an oven kept at 800 °C for 2 h in calm air. Subsequently, to assess the effect and the synergism of the noble metal over the carriers, Pd-based catalysts were prepared with a one-step route based on SCS: the same procedure previously described was employed, by simply adding $Pd(NO_3)_2$ to the precursors solution, in an amount corresponding to 2% in weight as noble metal load.

The ceramic oxides were characterized by X-Ray diffraction (PW 1710 Philips diffractometer equipped with a monochromator Cu Kα) to assess their purity and crystalline structure; the BET specific surface area was evaluated from the linear parts of the BET plot of the N_2 adsorption isotherms (Micromeritics ASAP 2010 analyzer); Scanning Electron Microscope (SEM/EDX LEO Supra 35, with an SUTW–sapphire detector) was employed to analyze the microstructure of the crystal aggregates.

The capability of the as-prepared catalysts to act as O_2 pumps was investigated by temperature programmed desorption (TPD) of O_2 (Termoquest TPD/R/O 1100, Series Thermo Finningan analyzer, equipped with a thermal conductivity detector TCD). A fixed bed of catalyst (about 250 mg in weight for each catalyst) was enclosed in a quartz tube and sandwiched between two quartz layers; then, an oxidation pretreatment was carried out by heating the fixed bed under 50 Nml min^{-1} of O_2 flow up to 900 °C at 10 °C min^{-1}. Then, after a 30 min stay at this temperature under O_2 flow, the reactor temperature was lowered down to room temperature under oxidizing atmosphere, thereby allowing for complete O_2 adsorption over the catalyst. Afterward, He was fed to the reactor at 25 Nml min^{-1} flow rate for 1 h at room temperature, thus purging out any O_2 excess. TPD tests were then performed by heating the catalyst up to 1100 °C at a rate of 10 °C min^{-1} under He flow. The O_2 desorbed during heating and present in the outlet flow was measured by the TCD detector after proper calibration.

The catalytic activity towards CH_4 oxidation of the as-prepared catalytic powders was tested in a lab-scale fixed-bed reactor: 0.1 g of catalyst (pressed in a pellet, crushed and sieved in the range 0.4–0.6 mm) mixed with 0.9 g of SiO_2 (0.3–0.7 mm in size, from Unaxis), sandwiched between two quartz wool layers, were inserted in a quartz tube (4 mm ID). The reactor, placed into a PID regulated electrical oven [16], was fed with 50 Ncm^3 min^{-1} of a gaseous mixture containing CH_4 (2%), O_2 (16%) and He (balance). The reactor temperature was measured by a K-thermocouple placed inside the catalytic bed. Starting from 800 °C, the oven temperature, was decreased at 2 °C min^{-1} rate and the outlet CO_2, CO, CH_4 and O_2 concentrations were determined by a NDIR continuous analyzer (Hartman & Braun URAS 10E), thus allowing to evaluate CH_4 conversion. By plotting CH_4 conversion vs the catalytic bed temperature it was possible to obtain the typical sigma-shaped conversion curves. The half-conversion temperature (T_{50}) was considered as an index of the powders catalytic activity.

2.2. Structured catalysts

A suitable deposition technique based on in situ SCS combined with the spray pyrolysis method was developed for the application of the catalysts on the metal fibre burners [7,8,16,17]. This technique can be considered as optimal one to guarantee a good adherence of the catalytic layer onto the metallic surface, preserving in the meantime the rapidity and low-cost characteristic of the SCS route.

The metal burners employed in the present study were manufactured with knitted fibre mats made of Fe–Cr–Al alloy, directly provided by Riello [27]. The knitted mats are very flexible products, suitable for any kind of burner geometry (e.g. flat, conical or cylindrical burner shape). The Fe–Cr–Al alloy possesses an outstanding resistance to high-temperature oxidation because of the formation of an α-Al_2O_3 protecting layer [28] that in this case, offers also a useful basement for anchoring the catalytic phase layer. As a first step, the metal burner mats were kept at specific temperature by flowing an O_2–N_2 mixture in order to favour the regular growth of α-Al_2O_3 grains into a uniform thin layer directly from the metal fibres [28], ensuring in the meanwhile an external surface morphology suitable for a good adherence of the catalytic phase to the metallic panels. Such pre-treated panels were then subjected to catalyst deposition.

Based on the results previously obtained on powders, all the investigated catalysts were employed: a first series without noble metal, i.e., $LaMnO_3$-ZrO_2, CeO_2-ZrO_2 and $BaCeO_3$-ZrO_2; a second series containing Pd as 2% in weight respect to the amount of deposited mixed oxides layers, i.e., 2% Pd/$LaMnO_3$-ZrO_2, 2% Pd/CeO_2-ZrO_2 and 2% Pd/$BaCeO_3$-ZrO_2. For each burner, a solution with the precursors of the metal oxides was prepared with distilled water, using glycine as fuel. Then the solution was sprayed over the surface of the pre-oxidized metal fibre mats, previously pre-heated at 450 °C [7]. Owing the in situ SCS-spray pyrolysis occurring on the hot panels, the catalytic synthesis was performed.

Subsequently, the fibre mats were placed back into the hot oven to stabilize the coating. The spray deposition cycle was repeated many times until the desired catalytic load (2 % wt) was reached. For further stabilization and complete crystallization of the catalytic phase, the coated fibres were finally calcined at 900 °C for 2 h in calm air. Pd on burners was added in a second step, by adopting the same deposition procedure: further spray-pyrolysis runs were performed over the perovskite or mixed oxides layer, by employing a diluted $Pd(NO_3)_2$ aqueous solution. Calcination in air at 600 °C then followed, to promote the full decomposition of $Pd(NO_3)_2$ into the oxidized form PdO [16].

SEM analyses (SEM/EDX LEO Supra 35, with an SUTW–sapphire detector) were carried out on all the prepared catalytic burners to evaluate the quality of the adherence and to verify whether the highly porous morphology observed with the catalytic powders was maintained after the deposition procedure; in this way, the effectiveness of the adopted deposition technique was ascertained. Attention was paid towards the coating uniformity and thickness; the presence of the desired perovskite/oxides phases was verified via EDX.

The as-prepared catalytic fibre burners and the non-catalytic counterpart were tested in a commercial domestic wall condensing boiler, with a nominal heat power of 35 kW, directly provided by Riello. The boiler was suitable for the production of both sanitary and heating water in household appliances. In the boiler, air (controlled by the electric fan) and CH_4 (controlled by an electro-valve) were premixed in the electric fan and then fed to a cylindrical shaped burner (D = 50 mm, length = 120 mm), made of catalyzed metal fibre mats, prepared as described above. The flue gases, cooled in a heat exchanger in which the water temperature was maintained stable from 30 °C (inlet) to 50 °C (outlet) at a constant pressure of 1.5 bar by a pump, were monitored by a multiple gas analyzer (a NO\NO$_2$\CO\CO$_2$ infrared analyzer and a O_2 paramagnetic sensor from ABB). Combustion tests were carried out by varying the operating conditions (i.e., the input power Q, from 10 to 35 kW, and the air excess E_a, related to the stoichiometric conditions, from 5% to 60%). Moreover, also the flame patterns (i.e., radiant, transition or blue flame regime) were checked through a peep hole on the combustion chamber. The burner is shown in Fig. 1.

Fig. 1. Photography of the premixed metal fibre burner.

3. Results and discussion

3.1. Catalytic powders

The XRD diffraction patterns of the as-prepared catalytic powders (not reported here, but visible in [29–31]) showed that all the catalysts obtained by SCS presented a good crystalline degree. When the $LaMnO_3$ catalyst was co-synthesized with ZrO_2 in a ratio 1:2, the $LaMnO_3$ preserved its perovskite structure (orthorhombic one), and the ZrO_2 phase appeared in an intimate mixture with the perovskite. The CeO_2 co-synthesized with ZrO_2 in a stoichiometric ratio 1:2 changed the oxide crystalline lattice from the cubic form of the initial simple oxide to the tetragonal lattice of the $Ce_2Zr_3O_{10}$ compound in which the molecular ratio between CeO_2 and ZrO_2 is 2:3. As concerns the $BaCeO_3$ co-synthesized with ZrO_2 in a molecular ratio 1:2, the peaks of the diffraction patterns were attributed to two different species: in particular Zr went into the B site of the initial perovskite (general formula ABO_3) forming a new phase, $BaZrO_3$ (cubic structure), with a complete Ce substitution in the B site; the expelled Ce gave rise to the crystallized $Ce_2Zr_3O_{10}$, as for the CeO_2-ZrO_2 mixed oxide system. Considering the spectra of the Pd-based catalysts, they were exactly equivalent to the respective counterparts without Pd; no diffraction peaks related to Pd were detected, a sign that Pd dispersion was satisfactory.

Table 1 shows the BET specific surface area values of the as-prepared powdered catalysts. The addition of Pd leaded to a loss of specific surface area, which was slight for $LaMnO_3$-ZrO_2 and CeO_2-ZrO_2 systems but appreciable for the $BaCeO_3$-ZrO_2 mixed oxide one.

The SEM analysis of the co-synthesized catalysts (Fig. 2) showed the typical spongy structure for $LaMnO_3$-ZrO_2 (Fig. 2A): the nanometric porosity obtained during the SCS preparation (and maintained during the calcination phase), responsible to the high BET values, is enlightened at high magnitude. The CeO_2-ZrO_2 system (Fig. 2B) presented a more compact morphology, with an interesting porosity of nanometric dimension, but with a lower BET s.s.a. value compared to $LaMnO_3$-ZrO_2. The $BaCeO_3$-ZrO_2 catalyst (Fig. 2C) evidenced a similar spongy morphology: the porosity, clearly visible at high magnitude, is however related to the micrometric scale, thus justifying the lower BET s.s.a. values obtained for this catalytic material (see Table 1). The morphological structures of the three catalysts were not modified by the addition of Pd.

Fig. 3 shows the TPC plots of CH_4 conversion (ζ_{CH4}) vs temperature; the one of SiO_2 is drawn for comparison. The addition of Pd lowered the T_{50} in all cases, even if in different extent (see Table 1). In particular, the Pd/CeO_2-ZrO_2, accounted for the maximum synergism between the noble metal and the mixed oxides; a T_{50} reduction of more than 100 °C compared to the CeO_2-ZrO_2 system was in fact recorded, whereas the T_{50} reduction for the other two catalytic systems, compared to their non-catalytic counterparts, was of 25 °C maximum. This fact could be explained considering that CeO_2-ZrO_2 system either acts as oxygen pump, owing to the potential of adsorbing O_2 on the surface and releasing it when in contact with reducing agents, or possesses the capability of changing the O_2 content in the crystalline lattice in combination with the valence variations of transition metals or lanthanides

Table 1
BET specific surface area and T_{50} values of the as-prepared powdered catalysts, with and without Pd.

Catalysts	BET s.s.a. [$m^2\ g^{-1}$]	T_{50} [°C]
$LaMnO_3$-ZrO_2	132.5	595
CeO_2-ZrO_2	81.4	490
$BaCeO_3$-ZrO_2	45.6	533
Pd/$LaMnO_3$-ZrO_2	132.0	570
Pd/CeO_2-ZrO_2	74.6	382
Pd/$BaCeO_3$-ZrO_2	26.4	512

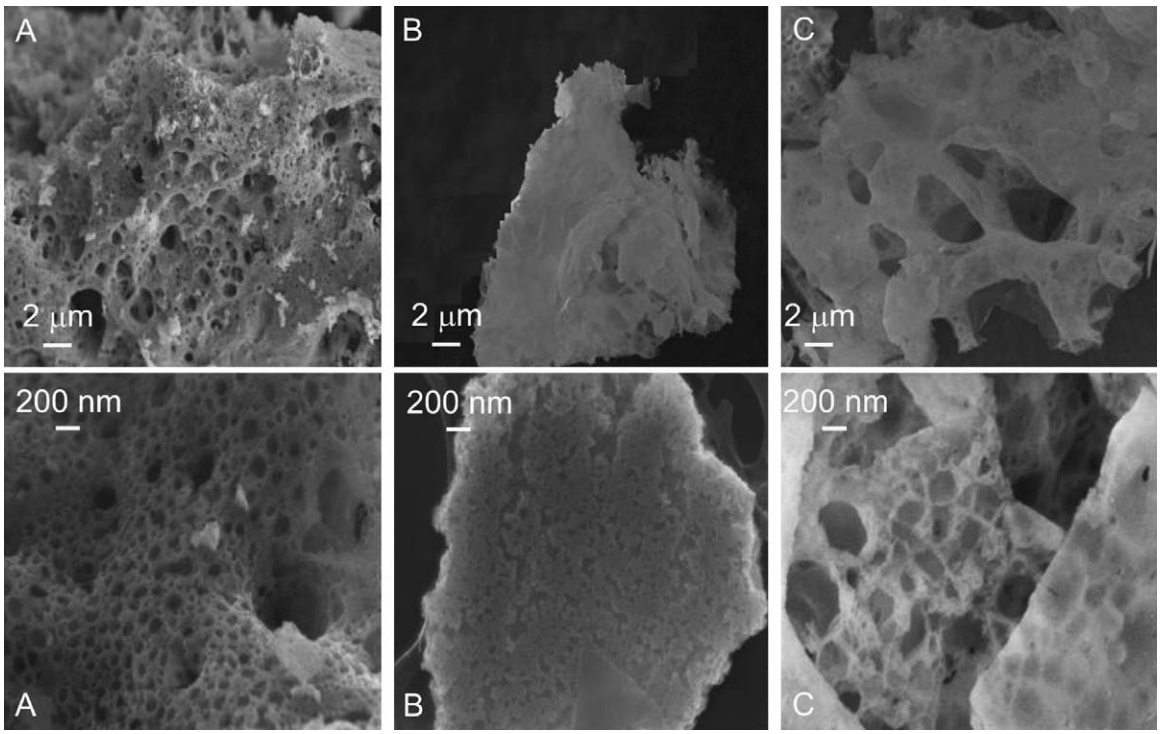

Fig. 2. SEM micrographs at different magnifications (5000× and 80,000×) of $LaMnO_3$-ZrO_2 (A), CeO_2-ZrO_2 (B) and $BaCeO_3$-ZrO_2 (C) powdered catalysts.

elements [32,33]. This is very helpful in the formation of the PdO species, known to be very active in CH_4 oxidation [34,35].

At powder level the most promising catalyst appeared to be Pd/CeO_2-ZrO_2, followed by Pd/$BaCeO_3$-ZrO_2 and Pd/$LaMnO_3$-ZrO_2.

The obtained O_2 TPD curves are drawn in Fig. 4. It is worth noting that Pd-based catalysts released higher O_2 moles per unit mass compared to their counterparts without Pd; this is in agreement with the lower T_{50} values recorded for the Pd-based catalysts during the TPC tests. The Pd/$LaMnO_3$-ZrO_2 catalyst desorbed the higher O_2 total amount (233.3 μmol g^{-1}), with the higher temperature peak (T_p = 960 °C) compared to Pd/$BaCeO_3$-ZrO_2 (128.7 μmol g^{-1} at T_p = 910 °C) and Pd/CeO_2-ZrO_2 (54.2 μmol g^{-1} at T_p = 535 °C). Considering 600 °C as the separation temperature between the released α- and β-O_2 [36], the Pd/CeO_2-ZrO_2 catalyst desorbed the highest amount of α-O_2 (46.1 μmol g^{-1}) compared to 16.2 and 0 μmol g^{-1} of Pd/$BaCeO_3$-ZrO_2 and Pd/$LaMnO_3$-ZrO_2, respectively, and its performance was better compared to the other two catalysts. It is well known [37] that CH_4 oxidation at low temperature occurs with a suprafacial reaction involving α-O_2. Therefore, from TPD and TPC tests it appears a tight link between the O_2 desorption temperature T_p (from TPD) and the catalytic activity of the catalysts (T_{50} TPC): the lower the T_p value, the higher the catalytic activity towards CH_4 combustion. The trend of T_{50} and T_p are indeed in close agreement.

To better understand the different performance of the studied catalysts, detailed FT-IR analysis on the powdered catalysts were performed and presented in [29–31]. Briefly, both Pd/CeO_2-ZrO_2 and Pd/$LaMnO_3$-ZrO_2 presented partly oxidized very small Pd metal particles and dispersed Pd oxide species [29]. Moreover, reduced Pd metal atoms resulted well dispersed on both supports, but some larger metal particles existed on Pd/$LaMnO_3$-ZrO_2 [30]. The coexisting very small Pd metal particles and Pd oxide species likely worked synergistically giving rise to high catalytic activity towards CH_4 combustion at low temperature. CH_4 activation, in fact, may be easier on Pd metal, Pd oxide providing oxygen species to form CO_2. The better performance of Pd/CeO_2-ZrO_2 compared to Pd/$LaMnO_3$-ZrO_2 could be ascribed to both the lower size of the Pd metal particles and the Pd partially reduced state more easily promoted from the electronic transition of Ce^{3+} ions [38].

Either Pd ions and support ions were detected also on Pd/$BaCeO_3$-ZrO_2 [31]; these species could be described as $Pd^{0/\delta+}$ species. In particular, an increased back bonding effect of the metal

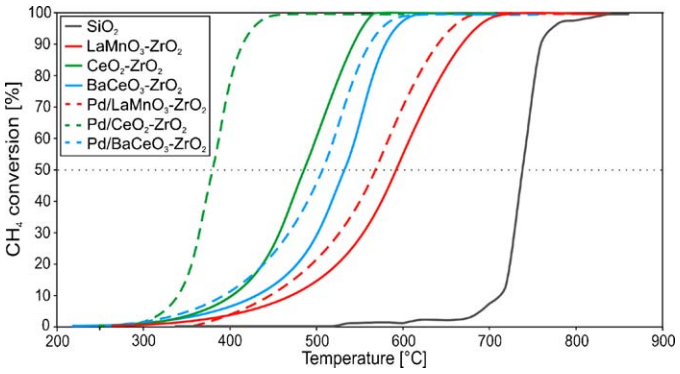

Fig. 3. CH_4-TPC plots of the as-prepared powdered catalysts.

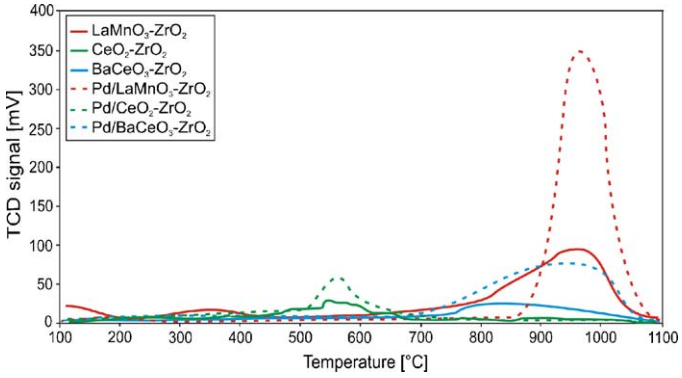

Fig. 4. O_2-TPD plots of the as-prepared powdered catalysts.

Pd particles from the basic oxygen anions of the support was noticed: such electron transfer from an electron donor (i.e., BaO) to metal Pd was also observed by other authors [25] via XPS analysis on Ba promoted Pd catalysts: a highly dispersed Pd metal phase was confirmed. However, the metallic Pd particles over Pd/$BaCeO_3$-ZrO_2 surface were larger in size compared to those on Pd/CeO_2-ZrO_2 [31]: this could suggest why the latter catalyst behaves better towards CH_4 combustion.

3.2. Structured catalysts

SEM analyses on structured catalysts (Fig. 5) showed very good results. The virgin fibres, of a cylindrical shape with approx 60–70 μm in diameter, appeared smooth (Fig. 5A). The pre-oxidation treatment allowed the growth of a very uniform and corrugated layer of α-Al_2O_3 (Fig. 5B): α-Al_2O_3 was strictly anchored to the fibres, with an average thickness evaluated as 1 μm, sufficient to host the catalyst. Fig. 5C (Pd/$LaMnO_3$-ZrO_2), 5D (Pd/CeO_2-ZrO_2) and 5E (Pd/$BaCeO_3$-ZrO_2) showed the morphology of the catalysts after the in situ SCS pray-pyrolysis deposition: in all cases, independently of catalyst, the layer appeared highly corrugated and porous. Therefore, the basic morphology of the powdered catalysts was preserved by the ad hoc developed deposition method. Moreover, on all the prepared catalytic mats, the catalyst layers were rather uniform all along the fibres, without cracks or fractures. EDX analysis confirmed the presence of the desired catalytic elements on the fibres.

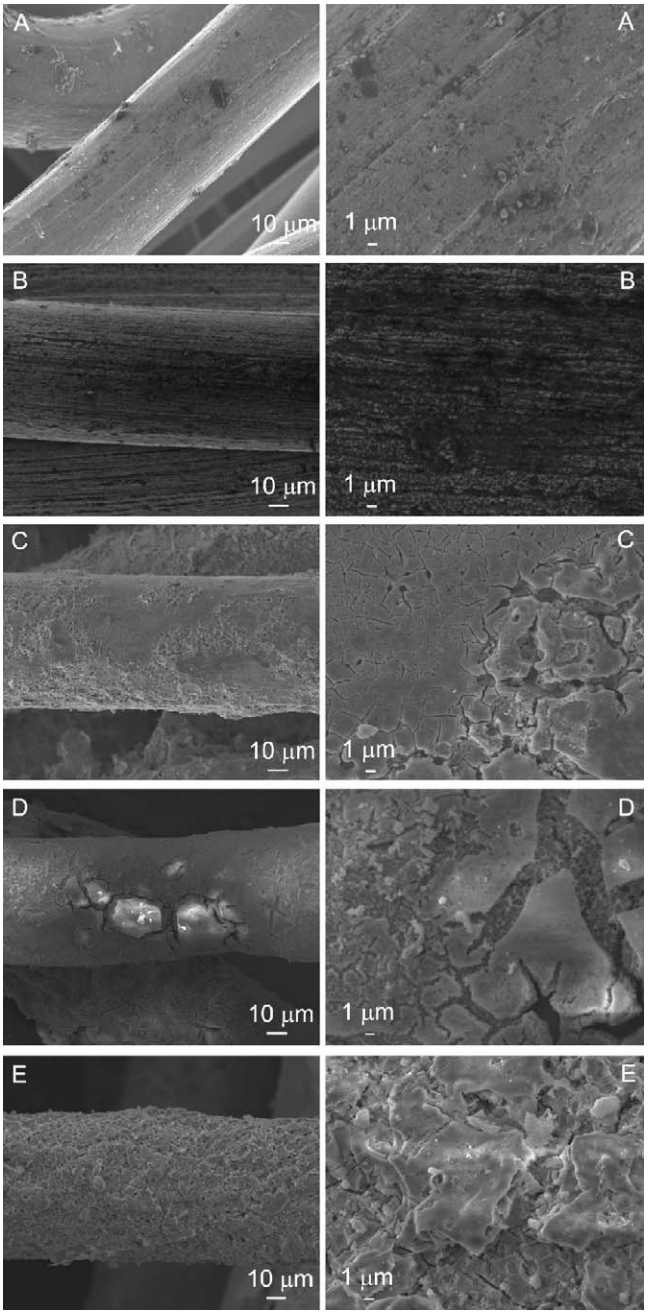

Fig. 5. SEM micrographs at different magnifications (1000× and 5000×) of the Fe–Cr–Al fibre mats: virgin (A); pre-oxidized (B); catalyzed with $LaMnO_3$-ZrO_2 (C); catalyzed with CeO_2-ZrO_2 (D); catalyzed with $BaCeO_3$-ZrO_2 (E).

The main results related to the burners' performance without the presence of Pd are shown in Figs. 6A and 7A as CO and NO emissionss released vs Q at three different E_a values: 5, 20 and 40% as minimum, medium and maximum air excess, respectively. The obtained values were compared to those obtained with the commercial burners usually assembled on the domestic boiler (gray curves in the figures).

As general comments, by increasing at constant E_a the burner heating power Q, i.e., the fuel feed rate, the CO emission levels increased, whereas the NO emissions curves presented a maximum, very marked at the minimum E_a value and practically lacking at the maximum one. By increasing the air excess, i.e., the air–methane ratio, CO and NO emissions were considerably lowered, mainly as a consequence of the air increase dilution effect (over-stoichiometric conditions), favouring on the one hand the complete CH_4 combustion and lowering on the other hand the flame temperature, thus limiting the formation of thermal NO_x (Zeldovich mechanism).

The catalysts performance order as concerns CH_4 combustion obtained at the powder level was confirmed at the structure state, too. In particular CeO_2-ZrO_2 and $BaCeO_3$-ZrO_2, worked very well in reducing the CO emissions at very low E_a in the whole heat power range (see E_a = 5%, Fig. 6A, where the combustion conditions were difficult due to the rather low excess of air). On the contrary, at the same conditions, NO emissions (see E_a = 5%, Fig. 7A) increased compared to the commercial burner (maximum increase of about 40%), by worsening the burners performance. In particular, CeO_2-ZrO_2 and $BaCeO_3$-ZrO_2, the best catalysts for CO abatement, were the worse ones compared to $LaMnO_3$-ZrO_2.

At high air excess operating conditions, the catalyst, independently from the composition, induced a very limited improving effect on the CO emissions level (see E_a = 20 and 40%, Fig. 6A) compared to the commercial burner. At these conditions, compared to the commercial burner, NO emissions increased in a lesser extent at the medium E_a value (maximum increase of about 20%, see E_a = 20%, Fig. 7A), and decreased a bit at the maximum E_a value (see E_a = 40%, Fig. 7A).

To better point out the role of catalysts on NO missions, Fig. 8A showed NO emissions data drawn vs E_a at three different Q levels: 10, 22 and 35 kW, assumed as minimum, medium and maximum tested values, respectively: at high E_a, higher than 30%, all the 3 tested catalytic burners reduced in a very limited extend (less than 10%) the NO emissions, whereas at low E_a, lower than 30%, the NO emissions increased compared to the commercial burner.

The situation was different for the catalytic burners when Pd was added: the trend remained similar to the catalytic burners without Pd, but the values reached in terms of CO and NO emissions were much more satisfactory. CO emissions (see Fig. 6B), lowered in all the examined conditions, especially at very low E_a (Fig 6B, E_a = 5%, compared with the corresponding Fig. 6A). Moreover, also at higher E_a values the catalytic effect was more appreciable compared to the burners without Pd. CO emissions were not only lowered, but also maintained a more stable trend

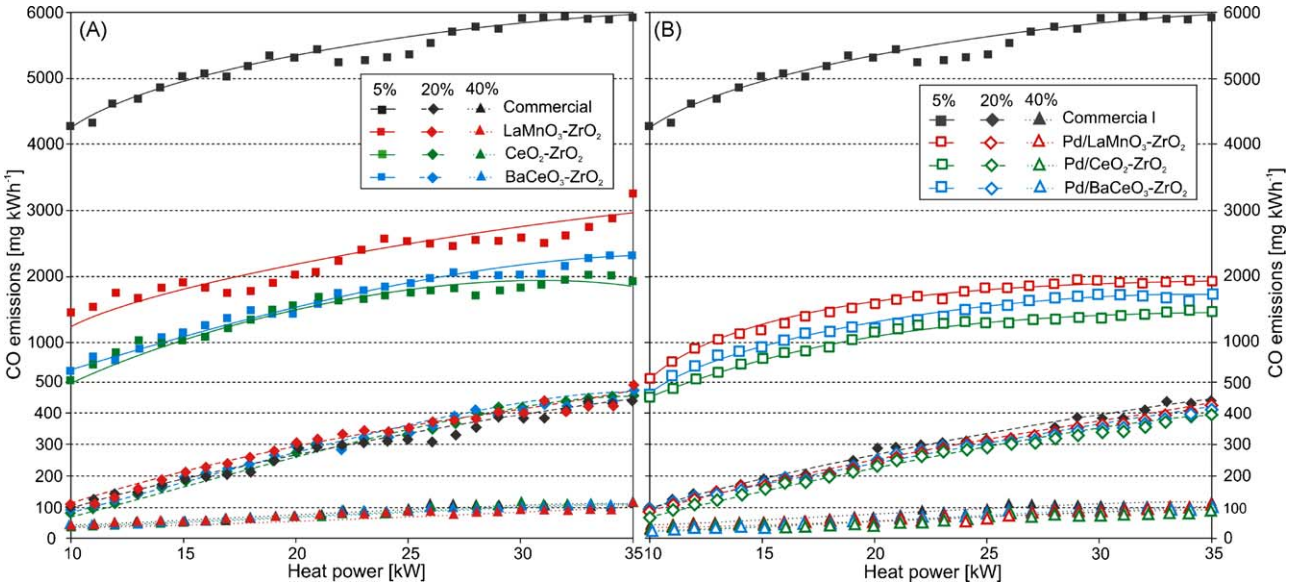

Fig. 6. CO emissions vs heat power Q at different E_a values: (A) catalytic burners without Pd; (B) catalytic burners with Pd.

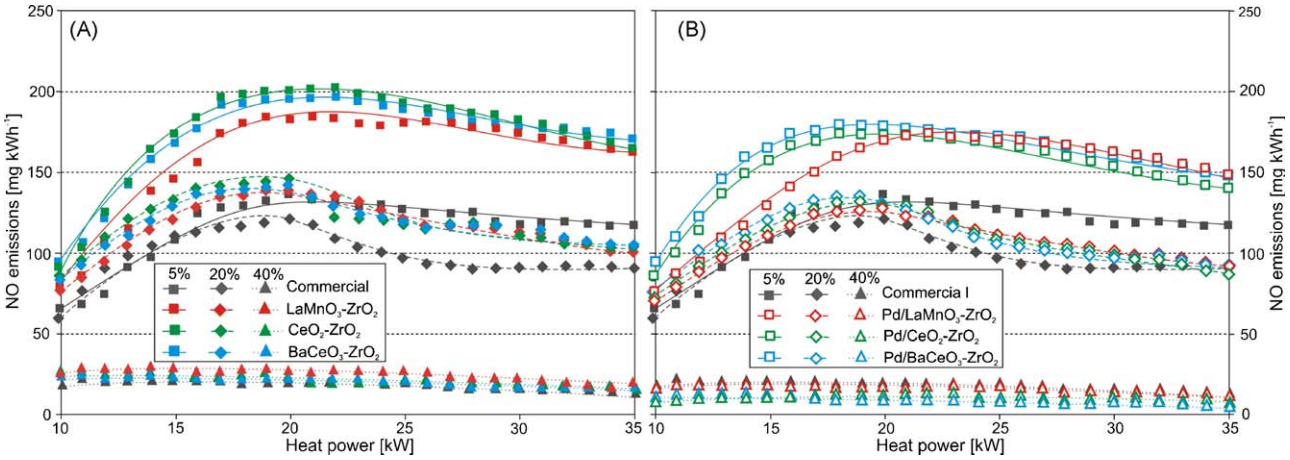

Fig. 7. NO emissions vs heat power Q at different E_a values: (A) catalytic burners without Pd; (B) catalytic burners with Pd.

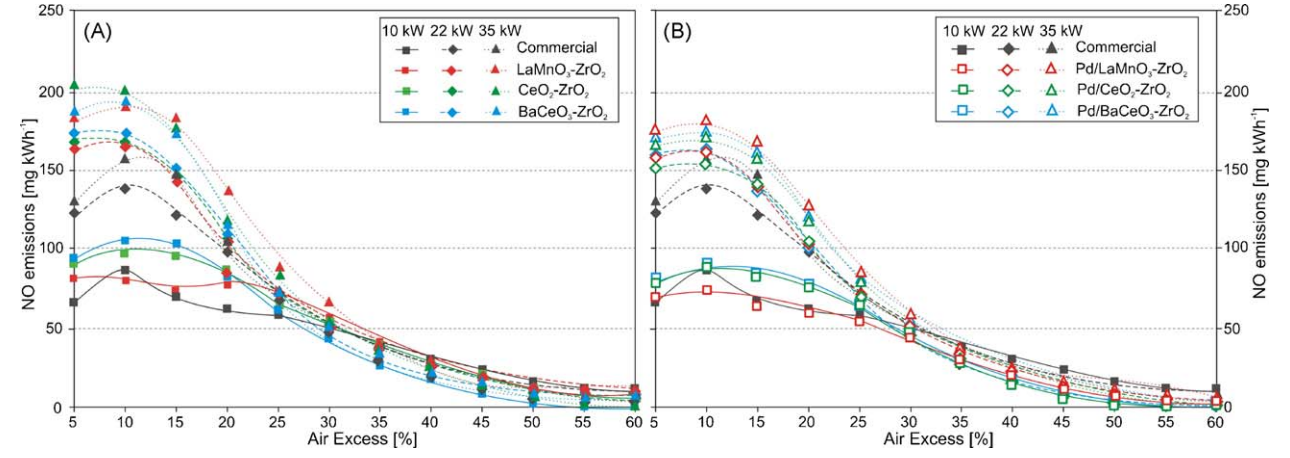

Fig. 8. NO emissions vs E_a at different Q values: (A) catalytic burners without Pd; (B) catalytic burners with Pd.

(the emissions curves appeared more linear, without oscillations). Pd/CeO_2-ZrO_2 burner performed better than $Pd/BaCeO_3$-ZrO_2 and $Pd/LaMnO_3$-ZrO_2, respectively, as demonstrated also at powder level as concerns CH_4 conversion (see Fig. 3).

Concerning the NO emissions, Pd-based burners improved the situation compared to the catalytic burners without Pd. As evident from Figs. 7A and B and 8A and B, NO emissions were lowered in all the tested conditions, but at low E_a values (from 5% to 20%, see Fig. 8A

and B), they were always slightly higher compared to the commercial burner, whereas at high E_a values (>30%) they were slightly lower. Here again, it is worth to notice that at low E_a, Pd/$LaMnO_3$-ZrO_2 burner worked better than Pd/CeO_2-ZrO_2 and Pd/$BaCeO_3$-ZrO_2 ones (the two latter absolutely equivalent in terms of performance), a result exactly opposite respect to the CO emissions.

NO_2 was practically absent in all the tested conditions, for all the burners.

3.3. Burners combustion regimes

As generally recognized, depending on the thermo-physical properties of the porous medium (permeability, emissivity, conductivity, etc.) and on the operating conditions (heat power Q and air excess E_a), two different combustion regimes can be established: the radiant and the blue-flame modes. The radiant regime, typically occurring at low both Q and E_a values, is characterized by a homogeneously red colour of the burner deck, a consequence of the high temperatures reached (800–1000 °C) by the porous mat surface downstream the reacting gases flow. Comparatively low NO_x emissions are expected in this regime, whereas rather high CO concentrations are encountered, especially at very low E_a values. In the blue flame regime, established at high Q and low E_a values (rich mixtures) or low Q and high E_a (lean mixtures), i.e., when the gas momentum inside the porous burner is comparatively high, a carpet of blue flames covers the burner deck leaving the porous mat comparatively cold. Higher NO_x emissions but lower CO emissions are typically encountered in this operating mode compared to the previous one, except at very low E_a values, where NO_x and CO emissions are higher. For average Q and E_a values, the burner is characterized by the co-existence of radiating and blue flame regimes (commonly named transition mode), distributed by spots on the burner deck.

Fig. 9A and B shows for each burner (commercial and catalyzed) the map of the observed combustion regimes with the smoothed curves of the first evolution from the radiant to the transition regime (lower group) and of the second one from the transition to the blue flame regime (upper group). Compared to the commercial burner, the presence of the catalysts reduced the transition regime area enlarging both the radiant (raising of the lower lines) and the blue flame zones (lowering of the upper lines). This is valid in particular for catalysts Pd/$LaMnO_3$-ZrO_2, and Pd/CeO_2-ZrO_2; in a lesser extent, especially for the radiant mode, for the Pd/$BaCeO_3$-ZrO_2.

Two opposite phenomena could explain these results. On the one hand, the deposited catalyst caused a certain increase in the gas momentum as a result of somehow reduction of the mat void fraction [17], thus increasing the gas path tortuosity; especially at high temperatures, the gas expansion combined with the reduced porosity results in an enhanced local gas momentum, which pushes the flame outside the burner deck. On the other hand, the presence of the catalyst can stabilize at least part of the flame front within the porous media by promoting in advance the CH_4 oxidation. At low Q, the latter phenomenon prevailed: CH_4 combustion was more effectively assisted by the catalyst, also as the result of a higher residence time inside the burner, and the E_a increase did not cause an immediate shift into the transition mode. At high Q, instead, the combustion mode could easily shift from the transition to blue flame regime, owing the prevalence of the former phenomenon. Moreover, the local gas momentum was further enhanced by the E_a increase.

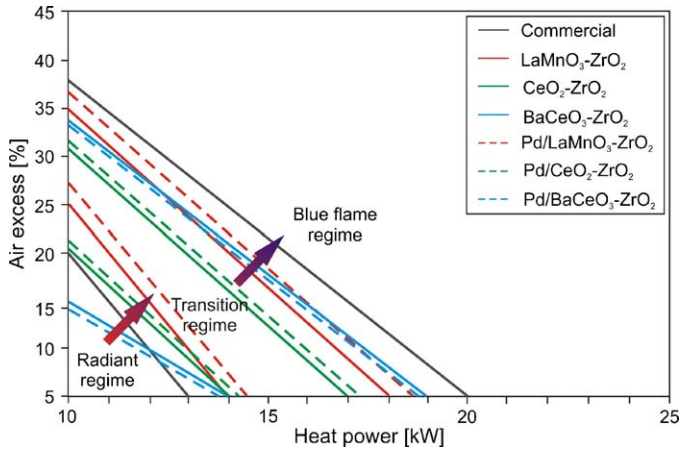

Fig. 9. Combustion regimes map: E_a vs Q.

With the catalyst promoting in advance the fuel oxidation, a greater portion of the combustion heat can be released within the porous medium, thus increasing its temperature, its radiant output and the overall thermal efficiency. If the catalyst can stabilize the combustion reactions deeper inside the metal fibre mat, the gas phase is cooled by the porous medium that absorbs and radiates directly to the heat sink. The consequent gas lower temperature could play favourably in containing the thermal NO_x formation: this was indeed confirmed by the experimental results, where the more efficient Pd-based catalysts, able to reduce more the CO emissions respect to the burners without Pd, allowed a greater reduction of NO_x emissions.

4. Conclusions

New catalytic material based $LaMnO_3$-ZrO_2, CeO_2-ZrO_2 or $BaCeO_3$-ZrO_2, without and with Pd, were developed through a fast and relatively cheap technique, the solution combustion synthesis, allowing to successfully synthesize catalysts with high specific surface area, good degree of purity and interesting catalytic activity towards CH_4 oxidation at powder level. By adopting the in situ SCS combined with the spray pyrolysis as deposition technique, the above catalysts were subsequently used to prepare catalytic premixed fibre burners for household appliances, characterized by a lower environmental impact mainly in terms of CO emissions.

The obtained results with the Pd-based catalytic burners in terms of CO emissions showed better performances compared with those of the commercial one over a wide range of operating conditions; the NO emissions, however, resulted somehow increased, especially at the low thermal power and air excess, whereas slightly decreased at high air excess. The most interesting results in terms of CO emission reduction compared to the commercial burner were obtained in particular with the Pd/CeO_2-ZrO_2 catalyzed burner. Further activities are in progress to better understand such phenomena and to study any hydro-thermal ageing and sulphur poisoning effects. These catalysts are particularly promising; in fact, it was demonstrated that 2% Pd/$LaMnO_3$-ZrO_2 and 2% Pd/$BaCeO_3$-ZrO_2 powdered catalyst when exposed to prolonged S-compounds ageing behave better than in the fresh status (i.e., their T_{50} decreased with ageing, [29,31]), whereas 2% Pd/CeO_2-ZrO_2 performance slightly decreased with ageing. Instead, still more interesting especially on an industrial point of view, the 2% Pd/$LaMnO_3$-ZrO_2 catalyst in the structured form (on the fibre mat) improved its performance compared to the commercial burner, both in terms of CO and NO_x pollutant emissions, when exposed to the same long-term S-ageing treatment of the powdered counterparts [8].

References

[1] P.E. Grohnheit, B.O. Gram Mortensen, Energy Policy 31 (2003) 817.
[2] Z.R. Ismagilov, M.A. Kerzhentsev, Catal. Rev. Sci. Eng. 32 (1990) 51.
[3] P. Forzatti, G. Groppi, Catal. Today 54 (1999) 165.
[4] S. Ro, A. Scholten, Catal. Today 47 (1999) 415.

[5] F.J. Cadete Santos Aires, S. Ramirez, G. García Cervantes, E. Rogemond, J.C. Bertolini, Appl. Catal. A: Gen. 238 (2003) 289.
[6] K. Qiu, A.C.S. Hayden, Fuel 85 (2006) 1094.
[7] S. Specchia, A. Civera, G. Saracco, Chem. Eng. Sci. 59 (2004) 5091.
[8] S. Specchia, M.A. Ahumada Irribarra, P. Palmisano, G. Saracco, V. Specchia, Ind. Eng. Chem. Res. 46 (2007) 6666.
[9] H. Sadamori, Catal. Today 47 (1999) 325.
[10] B. Emonts, Catal. Today 47 (1999) 407.
[11] B. Collongue, E. Garbowski, M. Primet, J. Chem. Soc. Faraday Trans. 87 (1991) 2493.
[12] T.V. Choudhary, S. Banerjee, V.R. Choudhary, Appl. Catal. A Gen. 234 (2002) 1.
[13] V. Dupont, S.-H. Zhang, R. Bentley, A. Williams, Fuel 81 (2002) 799.
[14] T. Seyama, Catal. Rev. Sci. Eng. 34 (1992) 281.
[15] S. Cimino, R. Pirone, L. Lisi, Appl. Catal. B: Environ. 35 (2002) 243.
[16] A. Civera, G. Negro, S. Specchia, G. Saracco, V. Specchia, Catal. Today 100 (2005) 275.
[17] S. Specchia, A. Civera, G. Saracco, V. Specchia, Catal. Today 117 (2006) 427.
[18] C.A. Müller, M. Maciejewski, R.A. Koeppel, A. Baiker, J. Catal. 166 (1997) 36.
[19] P. Fornasiero, G. Balducci, J. Kašpar, S. Meriani, R. Di Monte, M. Graziani, Catal. Today 29 (1996) 47.
[20] M. Boaro, M. Vicario, C. de Leitenburg, G. Dolcetti, A. Trovarelli, Catal. Today 77 (2003) 407.
[21] M.L. Pisarello, V. Milt, M.A. Peralta, C.A. Quercini, E.E. Mirò, Catal. Today 75 (2002) 465.
[22] M.M.A. Sekar, S.S. Manoharan, K.C. Patil, J. Mater. Sci. Lett. 9 (1990) 1205.
[23] K.C. Patil, S.T. Aruna, S. Ekarmann, Curr. Opin. Solid State Mater. Sci. 2 (1997) 158.
[24] L.F. Liotta, A. Macaluso, G.E. Arena, M. Livi, G. Centi, G. Deganello, Catal. Today 75 (2002) 439.
[25] F. Klingstedt, H. Karhu, A. Kalantar Neyestanaki, L.-E. Lindfors, T. Salmi, J. Väyrynen, J. Catal. 206 (2002) 248.
[26] S.R. Jain, K.C. Adiga, V.R.P. Verneker, Comb. Flame 40 (1981) 71.
[27] G. Toniato, A. Zambon, A. Lovato, M. Tomasetto, G. Mazzacavallo, La Termotecnica 2 (2006) 95.
[28] D. Ugues, S. Specchia, G. Saracco, Ind. Eng. Chem. Res. 43 (2004) 1990.
[29] S. Specchia, E. Finocchio, G. Busca, G. Saracco, V. Specchia, Catal. Today 143 (2009) 86.
[30] S. Specchia, E. Finocchio, G. Busca, P. Palmisano, V. Specchia, J. Catal. 263 (2009) 134.
[31] S. Specchia, P. Palmisano, E. Finocchio, G. Busca, Chem. Eng. Sci., in press doi:10.1016/j.ces.2009.05.007.
[32] G. Balducci, P. Fornasiero, R. Di Monte, J. Kašpar, S. Meriani, M. Graziani, Catal. Lett. 33 (1995) 193.
[33] P. Fornasiero, G. Balducci, R. Di Monte, J. Kašpar, V. Sergo, G. Gubitosa, A. Ferrero, M. Graziani, J. Catal. 164 (1996) 173.
[34] P. Briot, M. Primet, Appl. Catal. 68 (1991) 301.
[35] R.J. Farrauto, J.K. Lampert, M.C. Hobson, E.M. Waterman, Appl. Catal. B: Environ. 6 (1995) 263.
[36] Y. Teraoka, M. Yoshimatsu, N. Yamazoe, T. Seyama, Chem. Lett. 13 (1984) 893.
[37] M.A. Peña, J.L.G. Fierro, Chem. Rev. 101 (2001) 1981.
[38] E. Finocchio, M. Daturi, C. Binet, J.C. Lavalley, G. Blanchard, Catal. Today 52 (1999) 53.